Building and Environment 289 (2026) 114084

Contents lists available at ScienceDirect

Building and Environment

journal homepage: www.elsevier.com/locate/buildenv

Experimental investigation of supplied flow characteristics under impinging jet ventilation systems with round duct supply terminal

Haruna Yamasawa [a,*], Tomohiro Kobayashi [a], Toshio Yamanaka [a], Narae Choi [a], Moe Koshida [b]

[a] The University of Osaka, 2-1 Yamadaoka, Suita, Osaka, 565-0871, Japan
[b] TAKENAKA CORPORATION, 1-13, 4-chome, Hommachi, Chuo-ku, Osaka, Japan

ARTICLE INFO

Keywords:
Impinging jet ventilation
Full-scale experiment
Velocity profile
Particle image velocimetry

ABSTRACT

Using the impinging jet ventilation system (IJV), it is possible to accomplish high ventilation effectiveness within the occupied zone. Since the supplied air spreads along the floor, the flow feature is assumed to have a large impact on the whole room environment. To understand this, the jet's velocity profile was measured using a hotwire anemometer under isothermal conditions and particle image velocimetry (PIV) under isothermal and cooling conditions. Firstly, the velocity and turbulence intensity of the supply jet were measured to be around 2.8 m/s and 9.8%, respectively. Secondly, the maximum velocity decay and jet half-width expansion were shown. Thirdly, the relationship between measured dimensionless radial velocity and dimensionless height was shown to have a good agreement with Verhoff's equation and the free turbulent jet's equation in most of the regions, regardless of the angle from the wall. Fourthly, the velocity profiles at the central cross-section measured by the hotwire anemometer and PIV are almost the same in the region sufficiently far from the supply duct. Finally, the velocity profiles under isothermal and cooling conditions measured by PIV were practically the same; therefore, it is assumed that the findings listed above can also be applied to cooling conditions as well.

1. Introduction

Since HVAC occupies a large portion of the energy usage in the building sector, it is important to install a system with high ventilation effectiveness. One of the examples of a high-ventilation effectiveness system is the impinging jet ventilation system (IJV) [1]. In IJV, the air is supplied through the duct toward the floor, and once the air impinges on the floor, it moves along the floor (see Fig. 1) until the air is warmed up by heat sources. In this system, it is preferable that the sources of the contaminant and heat are the same; otherwise, the ventilation effectiveness may be compromised. After the supplied fresh air reaches the heat and contaminant source, the thermal plume around the source will move the heat and contaminant up to the upper region of the room. Therefore, a temperature and contaminant concentration gradient will be formed inside the room, and the air in the occupied zone is maintained fresh and cool.

Karimipanah et al. [2,3] introduced IJV by adopting the impinging jet to the ventilation field. Until then, the impinging jet itself was studied through theoretical and experimental approaches. The impinging jet's velocity profiles were reported by Bradshaw et al. [4] in 1959, Tsuei et al. [5] in 1963, Poreh et al. [6] in 1967, and Karimipanah et al. [7] in 1994. They reported measured results of the impinging jet flow characteristics and compared the findings across several geometrical configurations, such as radii, supply opening diameter, and supply velocity. When observing the jet after impingement, the flow features are expected to resemble those of a radial wall jet; therefore, it is valuable to review the research concentrating on its flow characteristics. The radial and two-dimensional wall jets were studied by Glauert [8] in 1956, Bakke et al. in 1957 [9], Verhoff in 1963 [10], and Tanaka in 1978 [11]. In addition, Rajaratnam [12] summarised the theoretical basis and experimental results of various jets, including impinging jets and wall jets, in his literature. Among all the research mentioned above, jet similarity is demonstrated, and some equations for the regression curves are introduced for the velocity profiles [8,10]. It must be noted that the

Abbreviations: IJV, Impinging jet ventilation; PIV, Particle image velocimetry; CFD, Computational fluid dynamics.

* Corresponding author.
E-mail addresses: yamasawa@arch.eng.osaka-u.ac.jp (H. Yamasawa), kobayashi@arch.eng.osaka-u.ac.jp (T. Kobayashi), yamanaka@arch.eng.osaka-u.ac.jp (T. Yamanaka), choi@arch.eng.osaka-u.ac.jp (N. Choi), koshida.moe@takenaka.co.jp (M. Koshida).

https://doi.org/10.1016/j.buildenv.2025.114084
Received 23 July 2025; Received in revised form 6 November 2025; Accepted 28 November 2025
Available online 29 November 2025

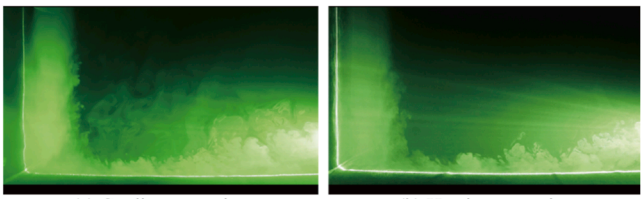

Fig. 1. Visualised impinging jet flow along the floor in the pilot experiment.

geometry of the openings and nozzles is not applicable (too small) for ventilation. Conversely, in atmospheric fields, Canepa et al. [13] reported the measured results of the impinging jet velocity of a downburst-like flow field through a scaled model experiment. However, its scale was too large for adoption in the ventilation field.

Karimipanah et al. [1] measured the velocity profiles along the floor of the IJV supply outlet. The supply outlet area was set to be 0.094 or 0.117 m^2, and the velocity profiles were measured at three angles: the planes, which are 30, 60, and 90 degrees from the wall. They introduced the equations for the maximum velocity decay and jet width expansion as a function of radial coordinate. Varodoumpun et al. [14] measured the vertical velocity profiles of an impinging jet discharged from a round duct with a diameter of 0.3 m. The measurement was conducted at the planes that are 0, 30, 60, and 90 degrees from the walls. The location of the supply outlet was also changed as a parameter (at the centre of the wall or the corner of the room). However, the number of measurement points in the vertical direction was limited so that the velocity decrease in the boundary layer was not captured in the experiment. They [15] also investigated the effect of inlet velocity profiles on the impinging jet velocity profiles by computational fluid dynamics (CFD).

Kobayashi et al. [16] measured the velocity profiles around the semicircular duct supply terminal with a diameter of 0.3 m mounted on a wall. The measurement was conducted using the I-type hot wire anemometer and 3D ultrasonic anemometer under non-isothermal conditions. The measured results were almost the same, and it was shown that the direction of the mainstream velocity vector was almost horizontal and radial at the measurement points farther than 0.4 m from the walls. Li et al. [17] investigated the jet flow feature of an air distribution system that supplies the air at the top of a cylindrical column from a doughnut-shaped slot outlet. They conducted a scaled-model experiment and measured the velocity along both the column and the floor by the 2D-PIV (particle image velocimetry) technique. They also compared the velocity profiles with the empirical equation for jet along the wall by Verhoff [10]. In addition, Yang et al. [18], Chen et al. [19,20] compared the impinging jet with different supply outlet shapes by CFD analysis. Han et al. [21] experimentally and numerically investigated the velocity profiles of wall-attached ventilation systems, who has a similar supplied air flow pattern.

After more than a decade since the introduction of the IJV's concept, the temperature distribution and ventilation effectiveness within the room have been actively studied to date. Additionally, the IJV is often compared with the displacement ventilation systems [22–26], another example of a high-ventilation effectiveness system. Nielsen proposed that those systems can be interconnected with each other by the idea of "family tree" [27]. The air distribution features of IJV were experimentally and numerically investigated in full-scale models in previous studies [1,16,28,29]. In addition, it was shown that IJV can prevent the over-cooling around the floor, while displacement ventilation has higher ventilation effectiveness.

Unlike displacement ventilation systems, IJV is known to apply to heating conditions due to the relatively large supply momentum. Yamasawa et al. [30] compared the heating performance and ventilation effectiveness between IJV and DV by a full-scale experiment. Ye et al. [31,32] presented that it is advantageous to install IJV rather than the mixing ventilation in terms of the heating efficiency. Ye et al. [33] also claimed that the warm air spreading distance in IJV will not exceed 12 m for any nozzles.

The indoor environment with IJV under both cooling and heating conditions has been studied in terms of ventilation effectiveness in the previous works [1,34–39]. On the other hand, the velocity profiles under different temperature settings have not been sufficiently studied by experiment to date, due to its difficulty in measuring. The supplied jet flow along the floor plays an important role in a room with an IJV. However, the studies that investigated the impinging jet flow feature as an air distribution system in a full-scale experimental setup under non-isothermal conditions [1,14,19,40] are still limited. Therefore, a more detailed experimental investigation is required to fully understand the jet flow features. In addition, not only the jet flow feature after the impingement, but also the velocity and turbulence statistics at the inlet duct are acquired as a reference for the boundary conditions when conducting CFD analysis. A full-scale experiment is conducted to obtain the velocity profiles of the impinging jet, and the results are discussed in the present paper.

To provide fundamental data for researchers investigating the indoor environment with IJV under both isothermal and cooling conditions, velocity measurements are carried out in a full-scale experimental chamber, and the velocity profiles along the floor are reported in the present paper. The present research mainly aims to (i) provide the turbulence statistics of the supply jet in IJV, (ii) understand the jet flow features at different cross-sections, and (iii) understand the jet flow features under different temperature settings. The hotwire anemometer was chosen to measure the velocity profiles under isothermal conditions owing to its accuracy and short time constant (Aim-(i) and (ii)). Meanwhile, the hotwire anemometer can cause some errors due to its measurement principle under non-isothermal conditions. The jet along the floor includes the area where the velocity and temperature fields change complexly over time. Therefore, it is difficult to measure the temperature and velocity of the jet flow simultaneously at the same place. Additionally, it is also difficult to measure the temperature with high frequency, as with velocity measurement. Therefore, in such environments, either temperature compensation must be applied, or an alternative measurement device must be chosen. (Aim-(iii)); hence, the PIV technique was carried out. The results obtained under different temperature settings using PIV are to be compared to understand whether the obtained results under isothermal conditions using the hotwire anemometer can also be applied for the cooling conditions. In addition, (iv) the difference in measured results among applied measurement techniques is to be discussed as well. Consequently, the measurement results by PIV will be validated by the hotwire anemometer under isothermal conditions, to support the findings in Aim-(iii).

2. Methodology

To understand the flow feature of the supplied jet in IJV, the velocity profile of the supplied jet moving along the floor is measured in a full-scale experimental chamber. As mentioned above, this paper aims to provide (i) the turbulence characteristic of the supply jet, (ii) understand the jet flow feature at different angles, and (iii) understand the jet flow feature under different temperature settings, i.e., whether the obtained results under isothermal conditions can also be applied to the cooling conditions or not. In addition, (iv) the velocity profiles obtained by a hotwire anemometer and PIV are to be compared as well.

The hotwire anemometer was chosen for the measurement under the isothermal condition to obtain a detailed and accurate velocity profile. However, given the possible experimental error caused by differences in temperature between measured and calibrated conditions, this equipment has a limitation for use under non-isothermal conditions if temperature compensation was not applied. Namely, the temperature compensation element is located at the back of the equipment; however, the airflow temperature around the probe can differ from that around the equipment. Therefore, due to this possible experimental error, the

particle image velocimetry (PIV) was chosen for the measurement under non-isothermal conditions, i.e., cooling conditions. To verify the accuracy of PIV, the PIV measurement was conducted under isothermal conditions as well. The results of the hotwire anemometer and PIV under isothermal conditions are to be compared and discussed in Section 3.

The vertical velocity profiles were measured at the plane that is perpendicular to a wall and passes through the centre of the wall (central cross-section). Karimipanah et al. [1] reported that the velocity profile varies depending on the angle from the wall; however, the number of measurement points was limited. Therefore, the velocity profiles were additionally measured at the planes that are 0°, 45° and 90° from the central cross-section (0°) by a hotwire anemometer with more dense measurement points than the previous study [1].

Section 2.1 describes the general room setups, Section 2.2 describes the velocity measurement methodology by hotwire anemometer under isothermal conditions over the supply plane and flow along the floor at different angles, and Section 2.3 describes the methodology of velocity measurement along the floor by PIV under non-isothermal conditions.

2.1. General room setups and experimental procedure

The measurement was conducted in an experimental chamber with a dimension of 5.00 × 5.45 × 2.77 (H) m, shown in Fig. 2. The experimental chamber is in the main laboratory, i.e., the chamber itself is located indoors so that the effect from the outdoor temperature is limited. As shown in the figure, there was another chamber (OC: outdoor chamber) next to the target chamber, which is for simulating the heat loss through the external wall in practice by changing the temperature inside. The air inside OC is warmed up under the cooling conditions, and the air-conditioning system (see Section 2.3 for details) is turned off under isothermal conditions. The wall between the target chamber and OC is insulated when conducting the measurement by hotwire anemometer, whereas it is not insulated when conducting the measurement by PIV under non-isothermal conditions. On the other hand, all the other walls were always insulated.

Inside the target chamber, a supply round duct with a diameter of 0.15 m was mounted in the centre of the wall on the OC side, and the height of the supply duct end was set to be 0.6 m above the floor. The supplied air flow rate was regulated using the volume damper, and the flow rate was estimated by the differential pressure between before and after the orifice flow meter (Iris damper, Continental Fan) installed at 1 m before the supply terminal. On the other hand, an exhaust outlet is mounted almost in the middle of the ceiling. The air-conditioned air is supplied through the supply duct with a ventilation rate of 180 m^3/h, which accounts for the mean velocity of 2.8 m/s through the supply inlet duct. The HVAC systems were maintained in the same condition for a sufficient time to obtain the steady-state velocity profiles.

2.2. Measurement by a hotwire anemometer under isothermal conditions

The measurement was first conducted using a hotwire anemometer with an I-type probe (0251 R-T5, Kanomax), where the obtained velocity is the composite velocity of two velocity components. The measurement data were stored in a data logger (NR-500, Keyence) at a frequency of 1.0 kHz for one minute, i.e., 60,000 data points for each measurement point. The measurement aimed to obtain the turbulence statistics at the supply jet (inlet boundary) and to understand the jet flow feature along the floor with different angles. The measurement points of the hotwire anemometer are shown in Fig. 3. The velocity profile of the supply jet inlet was measured at the central cross section, from −0.06 to 0.06 m from the centre of the duct at an interval of 0.01 m. Fig. 3(e) depicts the area used for calculating the area-weighted average of measured results. The methodology to calculate the turbulence statistics is summarised in Section 2.4.

The velocity profiles along the floor were measured at 0.2 - 1.0 m horizontally from the centre of the inlet duct in the radial direction, whereas, in the vertical direction, the measurement points are set at 0.002 - 0.2 m above the floor. Additionally, the velocity profiles were measured in the planes where 0°, 45°, and 90° from the central cross-section of the test chamber, and here, the planes are to be called Plane-00, Plane-45, and Plane-90, respectively.

The measurement setups were mounted on a 2D traverser and moved vertically and horizontally when changing position. However, to avoid the interaction of the target jet and the traverser, the traverser was set on a steel frame with four legs, as shown in Fig. 4. It must be noted that the measurement was conducted under an isothermal condition. The supplied air temperature was maintained at 22 °C, and the wall between the target chamber and OC was insulated by installing polystyrene foam on the wall in OC.

2.3. Measurement by particle image velocimetry (PIV) under non-isothermal conditions

The velocity profiles along the floor under both isothermal and non-isothermal conditions were measured using the PIV technique. It must be noted that the measurement was only conducted in the central cross-section. The experimental settings are summarised in Table 1. To simulate the heat loss through external walls during the measurement by PIV, the air temperature inside OC was controlled by using three oil heaters (Max 1.2 kW each) in OC under cooling conditions. Additionally, the air within OC was sufficiently mixed with five fans. The air temperature within OC was controlled to achieve an exhaust air temperature

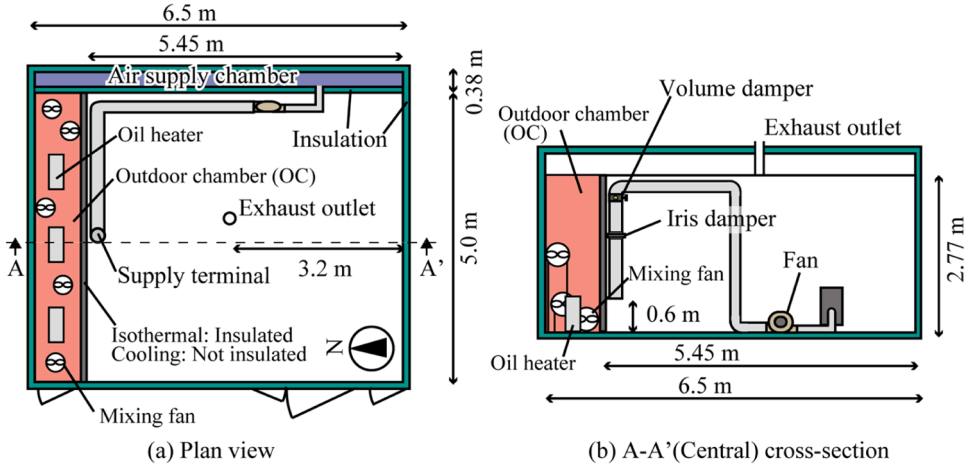

Fig. 2. Setups of the experimental chamber.

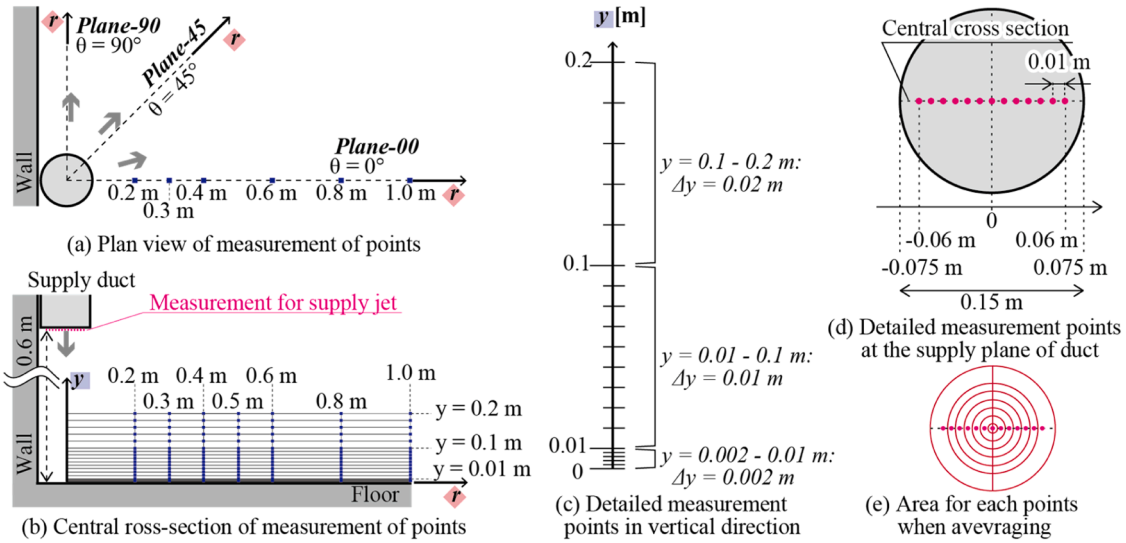

Fig. 3. Measurement points for hotwire anemometer.

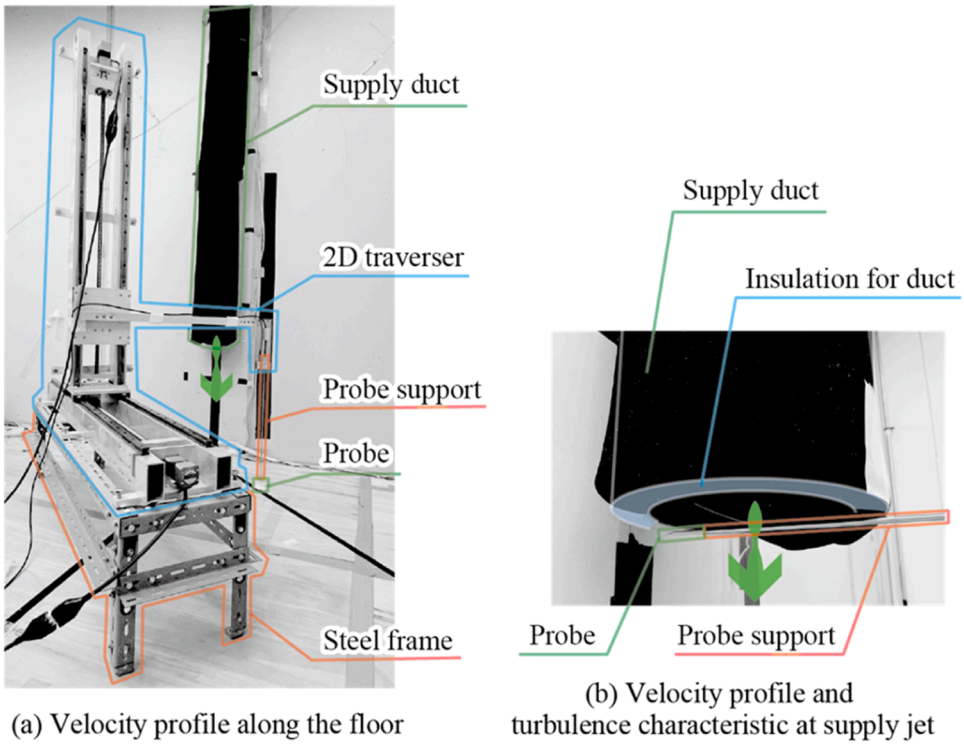

Fig. 4. Configuration of hotwire anemometer setups for each measurement.

Table 1
The temperature settings in each condition.

	Isothermal	Cooling
Supplied air	22.0 °C	20.0 °C
OC air	19.6 °C	35.6 °C
Exhaust air	21.9 °C	27.8 °C

to be around 27–28 °C under cooling conditions. On the other hand, the exhaust and supplied air temperatures were maintained at approximately 22 °C, which is consistent with the experiment with the hotwire anemometer. To achieve the conditions, the supplied air temperature is controlled at 22 °C and 20 °C under isothermal and cooling conditions, respectively.

The measurement setups for PIV are depicted in Fig. 5. The velocity profiles along the floor, extending from the vicinity of the inlet to 1.0 m away from the inlet duct centre, were obtained using PIV measurements. To achieve a detailed velocity profile around the supply terminal, the PIV system's CMOS camera was positioned close to the filming area; however, this results in reduced filming coverage and interaction with the target jet. Consequently, measurements were repeated at three positions, as illustrated in the figure, and the results at these three positions are connected in the final step. The filming coverage was adjusted to encompass an area of 0.43 × 0.57 m at the central cross-section. The camera was mounted on a 2D traverser and moved horizontally when changing position.

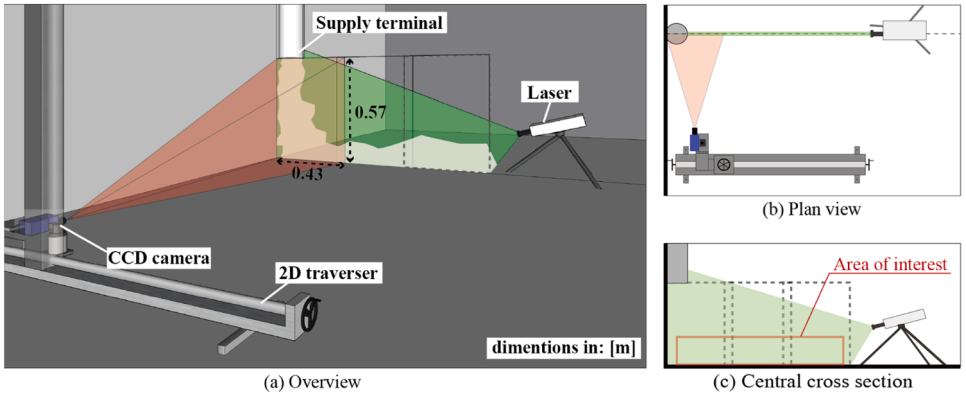

Fig. 5. Measurement setups of PIV.

The airflow was visualised by smoke injected in the vicinity of the supply terminal, while the airflow feature at the central cross-section was illuminated by a pulsed laser sheet. Table 2 provides a summary of the PIV measurement method. A double-pulse laser was controlled to irradiate twice within a short time interval (2.0×10^{-3} s), and a pair of photos of the visualised airflow was captured simultaneously by synchronizing the camera. Subsequently, the instantaneous velocity profile is analysed based on these two photos. The direct cross-correlation method [41–43] was applied for the analysis, employing the recursive correlation technique. By detecting a correlation peak within each interrogation window and averaging instantaneous velocity components calculated from a spatial shift within a known time interval, a 2-D time-averaged velocity profile was obtained. This data set was sampled every 0.1 s (frequency = 10 Hz) for 10 s; thus, 100 pairs of photos were collected each time. This process was repeated six times at the same location, and the mean velocity profile was derived by averaging these results over a total of 60 s.

Since the smoke was not injected into the supply terminal but into the ambient region, there was no smoke in the potential core. This strategy was adopted because the primary focus of the present experiment is the jet region along the floor after the impingement. The velocity profile of this jet could not be adequately analysed when the smoke was injected into the supply terminal during the pilot experiment (Fig. 1), despite the jet region along the floor being of interest. It seemed that the smoke was fully mixed in the duct and that there was no illuminance distribution within the potential core in the pilot experiment. Consequently, smoke was generated through aligned small tubes above the jet, as shown in Fig. 6, allowing the jet to induce the smoke, which leads to a non-uniform luminance distribution in the region of interest. However, it must also be noted that in the current experimental configuration, the mainstream of the supplied jet before impingement on the floor could not be visualised, as depicted in the figure.

Table 2
PIV measurement method.

Camera	Imager ProX 2 M, Lavision
Laser	Nd:YAG laser: DPIV-L50
Seeding	Smoke
Image size	1600 × 1200 pixels
Filming coverage	Approx. 0.57 × 0.43 m
Laser output	50 mJ/pulse
Sampling frequency	10 Hz
Sampling time	10 s × 6 times = 60 s in total
Time interval of double-pulse laser irradiance	2.0×10^{-3} s
PIV software	Davis 8.3
Method	Direct cross-correlation method
Interrogation window size	32 × 32 pixels
Overlap	50 %

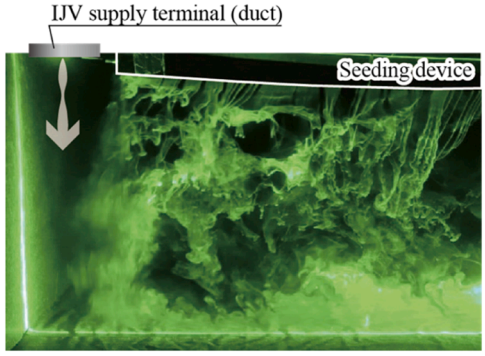

Fig. 6. Seeding of smoke for PIV around the supply terminal.

2.4. Calculation of turbulence statistics

The estimation method for the turbulence statistics (turbulence kinetic energy k, turbulence energy dissipation rate ε, specific dissipation rate ω, and turbulent length scale L) is briefly summarised in this section.

When a hotwire anemometer is used for the measurement, the measured velocity v has two components:

$$v^2 = {u_x}^2 + {u_y}^2, \tag{1}$$

where u_x and u_y are the velocities in the x and y directions. Here, the relationship between the Reynolds-average of squared fluctuating velocity components is assumed to be as follows:

$$\overline{v'^2} = \overline{{u_x'}^2} + \overline{{u_y'}^2}, \tag{2}$$

where V, U_x and U_y are the mean velocity components, v', u_x' and u_y' are the fluctuating velocity components. Although the turbulence is anisotropic, by adopting the assumption of isotropic turbulence, the turbulence kinetic energy k can be derived by [44]:

$$k = \frac{1}{2}\left(\overline{u_x'^2} + \overline{u_y'^2} + \overline{u_z'^2}\right) \approx \frac{3}{2}\overline{u_x'^2} \approx \frac{3}{4}\overline{v'^2}. \tag{3}$$

The turbulence intensity I_t, turbulence energy dissipation rate ε [45], and specific dissipation rate ω[45] are given by:

$$I_t = \frac{\sqrt{\overline{v'^2}}}{V}, \tag{4}$$

$$\varepsilon = C_\mu \frac{k^{3/2}}{L}, \tag{5}$$

$$\omega = \frac{\varepsilon}{C_\mu k}, \tag{6}$$

where C_μ is the model coefficient (= 0.09), and L is the turbulent length scale. The turbulent length scale is derived by assuming that it correlates to the mean velocity component and the characteristic time scale T, which is used to express the effect of the fluctuating velocity component [44]:

$$L = C_\mu^{1/4} VT. \tag{7}$$

The characteristic time scale is defined by integrating the autocorrelation function of the fluctuating velocity component $\rho(\tau)$ over time:

$$T = \int_0^\infty \rho(\tau) d\tau, \tag{8}$$

$$\rho(\tau) = \frac{\int_0^\infty v_t' v_{t-\tau}' dt}{\sqrt{\int_0^\infty v_t'^2 dt \int_0^\infty v_{t-\tau}'^2 dt}} \approx \frac{\int_0^\infty v_t' v_{t-\tau}' dt}{\int_0^\infty v_t'^2 dt}, \tag{9}$$

where t and τ are time. The derived turbulence statistics are reported in Section 3.1.

3. Results and discussions

The results are to be reported and discussed from four perspectives. Firstly, the fundamental data of the IJV supply jet: the velocity profile and turbulence statistics at the supply plane are provided in Section 3.1. Secondly, the angles: the velocity profiles at the plane in different angles from the central cross-section are compared in Section 3.2. Thirdly, the difference caused by measurement method and validation of PIV technique by hotwire anemometer: The velocity profiles along the floor obtained by a hotwire anemometer and PIV are to be compared and discussed in Section 3.3. Finally, the temperature settings: the effect of the temperature setting on the velocity profiles is discussed in Section 3.4.

3.1. Turbulence characteristic of the supply jet

The supply jet velocity and turbulence intensity measured by a hotwire anemometer are presented in Fig. 7, and the area-weighted averages of velocity and turbulence statistics are summarised in Table 3. It was found that the velocity profile was slightly asymmetrical. It is assumed that this is due to the configuration of the supply duct. The supply plane must be positioned further from the elbow to achieve a uniform profile. However, the coefficient of variation of the mean velocity and turbulence intensity is 3.9 % and 11.1 %, respectively, which does not seem to significantly affect the results. Here, the average value indicated in the diagram is shown as an area-weighted average value. However, since this non-uniformity is not significant, and the difference between the turbulence statistics listed in Table 3, derived from the arithmetic and area-weighted averages, was merely 0.06–2.44 %.

The average velocity is nearly the same as that calculated by the ventilation rate, i.e., 2.8 m/s. Since the supply terminal in the present study is a round duct, it was anticipated that the turbulent length scale would be approximately 0.07 times the diameter of the duct, i.e., 0.011 m. The estimated result based on the autocorrelation is 0.019 m, nearly double the expected value; however, the order remains the same. Therefore, it is considered that the turbulent length at the inlet boundary of the IJV round duct can be roughly estimated as 0.07D when conducting CFD analysis.

3.2. Jet flow features at different angles

The vertical profiles of radial velocity and turbulent kinetic energy in Plane-00, Plane-45, and Plane-90 measured by a hotwire anemometer are shown in Fig. 8. As the jet moves along the floor, the maximum velocity decays and the jet width stretches, which is widely known as the turbulent jet flow feature [12]. This feature was identical regardless of

Table 3
Area-weighted average of velocity and turbulence statistics at supply jet.

Mean velocity	Turbulence intensity	Turbulent kinetic energy	Turbulence energy dissipation rate	Specific dissipation rate	Turbulent length scale
V [m/s]	I_t [%]	k [m^2s^{-2}]	ε [m^2s^{-3}]	ω [s^{-1}]	L [m]
2.83	9.8	0.0574	0.0656	12.9	0.0189

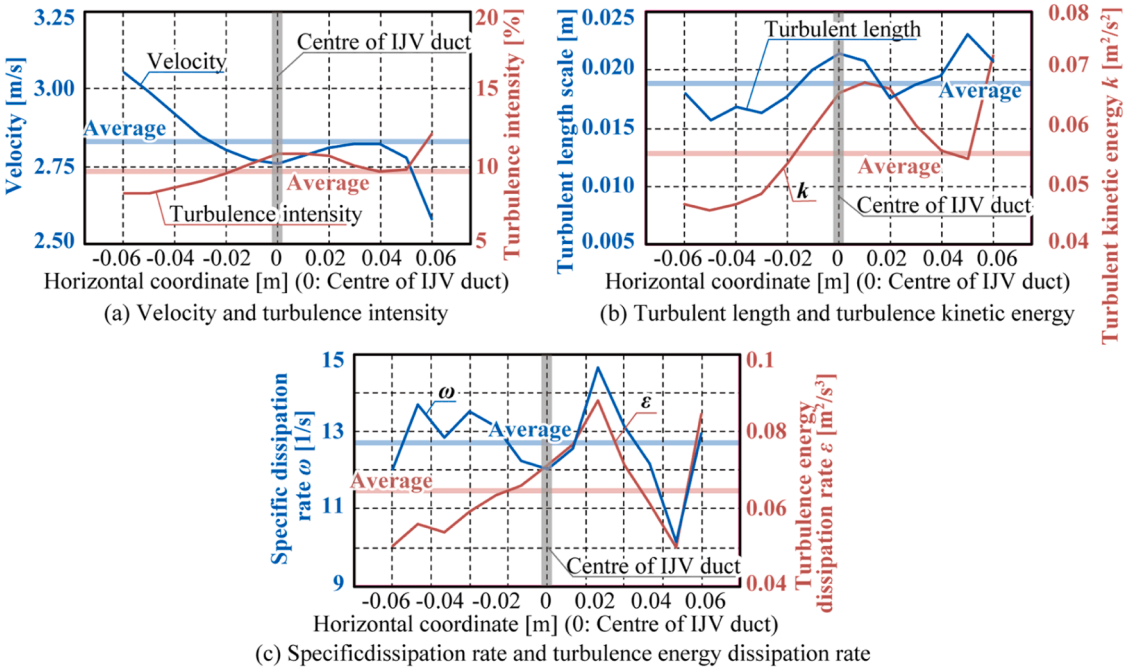

Fig. 7. Velocity and turbulence statistics profiles at the supply plane.

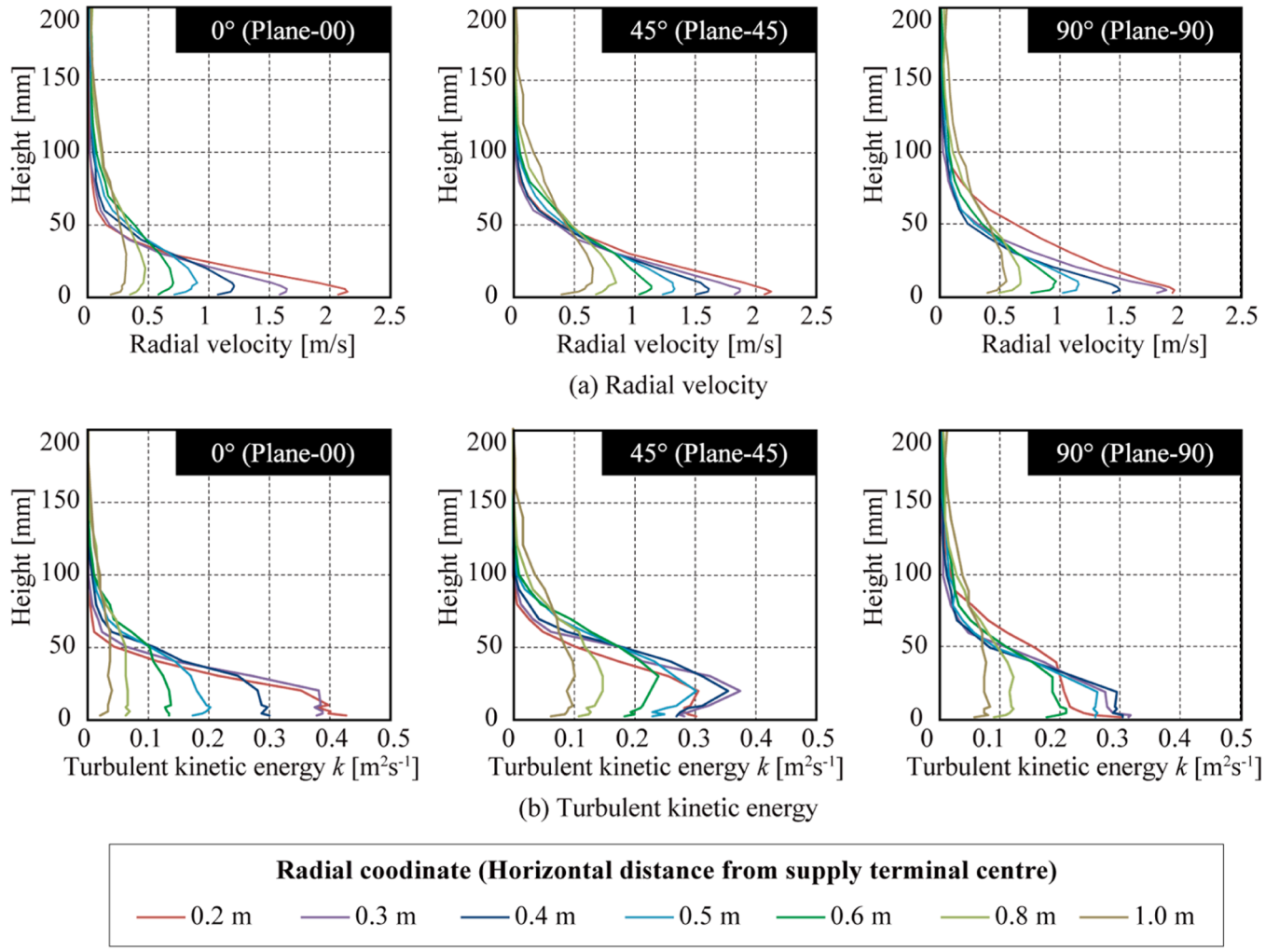

Fig. 8. The velocity and turbulent kinetic energy profiles at each radial coordinate at different angles.

the angle. It is also shown that the maximum velocity decay and jet width stretch are more significant at Plane-00 than at other planes. At Plane-90, the velocity profile (jet width) at the radial coordinate of 0.2 m is larger than the others, and the turbulent kinetic energy is smaller than at the other coordinates. However, as the jet spread, the jet rapidly lost this identity, and the velocity profile feature became like the others at the radial coordinate of 0.3 m. The flow feature around this region is to be discussed later in Section 3.3. In addition, the maximum velocity decay was more rapid in Plane-00 than in other planes, assumed to be due to the larger turbulent kinetic energy, which leads to the larger momentum diffusion correspondingly. The difference in turbulent kinetic energy profile is assumed to be affected by the vertical wall's

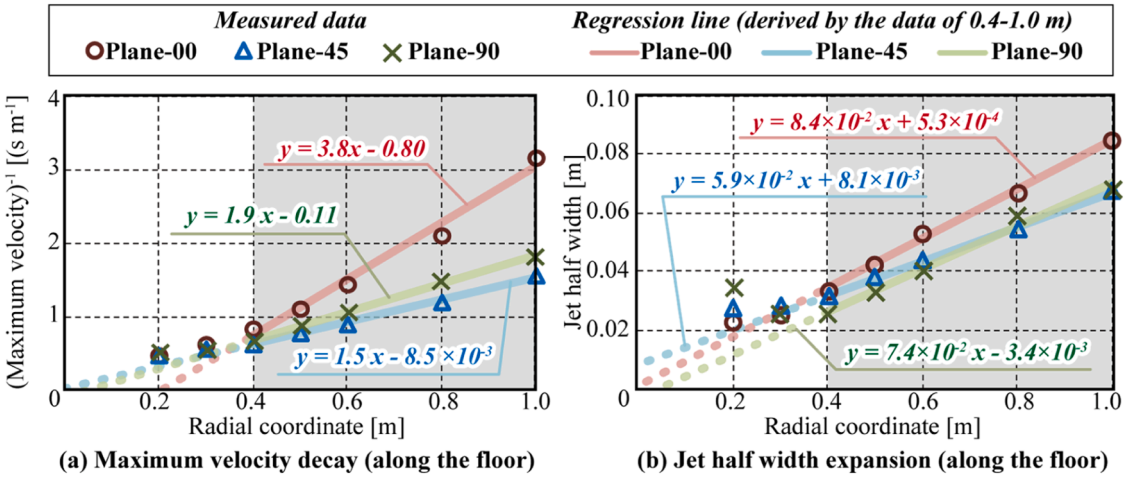

Fig. 9. The jet half-width expansion and maximum velocity decay along the radial coordinate.

restriction as well. It is assumed that the jet in Plane-90 not only has a vertical wall-jet profile from the wall as shown in Fig. 8(a) but also has a horizontal wall-jet profile from the vertical wall. This complicated configuration is assumed to have resulted in the derived velocity and turbulent kinetic energy profiles. It is suggested that a further measurement be conducted to understand this jet's restriction from walls.

To illustrate the difference by angle, the maximum velocity decay and the jet half-width expansion are shown in Fig. 9. It is known that the jet half-width is proportional to the radial coordinate while the maximum velocity is inversely proportional to the radial coordinate for a radial wall jet [12]. Therefore, the maximum velocity is shown in a reciprocal form.

The maximum velocity decreased, and the jet-half width expanded gradually in Plane-45 and Plane-90 compared to Plane-00 (the central cross section). It is assumed that a threshold exists at an angle between 0° and 45°, with this feature gradually changing from 45° to 90° This is likely due to restrictions from the wall; for example, the jet could spread upwards, right, and left in Plane-00, whereas it could only spread upwards and left in Plane-90. It is also suggested that the Coanda effect occurred on the wall surface, causing the jet to move along the wall as well. As a result, the vertical and horizontal spread of the jet around the central cross section leads to a relatively quick decay in maximum velocity (Vm), which causes a faster expansion of the jet-half width due to the smaller $0.5Vm$. The observations at Plane-45 are similar to those at Plane-90, and it appears that Plane-45 is influenced by Plane-90; however, the maximum velocity decay was slightly slower at Plane-45. It is possible that the airflow spreading from both sides maintained the maximum velocity at Plane-45, while friction between the jet and the wall reduced the maximum velocity around the wall.

The regression lines shown in Fig. 9 are derived using the data from the radial coordinate of 0.4 to 1.0 m, assuming that the jet is not sufficiently developed until 0.4 m away from the supply terminal centre. It was shown that the relationship between the vertical and horizontal coordinates is the same as the prior mentioned feature [12]. In other words, although the jet was restricted by the wall, the jet flow feature doesn't change significantly from the radial wall jet. The relationship between the radial coordinate and jet half width of the radial wall turbulent jet is expressed as a linear function by Bakke [12]. It is worth mentioning that the slope in the equation by Bakke is 7.8×10^{-2}, which is similar to that of the present paper.

Finally, the vertical profiles of radial velocity are shown in the dimensionless form in Fig. 10. The jet half-width (height) b and maximum radial velocity V_m are used as the reference for the height and radial velocity, respectively. The figure shows that this relationship can be expressed by an equation regardless of the angle. Verhoff et al. [10] introduced an equation to express the velocity profile of a 2-D jet along walls (Eq. (1)).

$$\frac{V}{V_m} = 1.48\left(\frac{y}{b}\right)^{1/7}\left[1 - erf\left(0.678 \times \frac{y}{b}\right)\right] \tag{10}$$

where, V is the velocity at each point, V_m is the maximum velocity, y is the height of the measurement point, and b is the jet-half width. On the other hand, he also claimed that this profile could be roughly expressed by a simpler equation for the free turbulent jet (Eq. (2)).

$$\frac{V}{V_m} = \exp\left[-C \times \left(\frac{y}{b}\right)^2\right] \tag{11}$$

where, C is a coefficient that must be determined by experimental data ($C = 0.637$ with RMSE = 0.058 m/s). Nevertheless, it must be noted that when comparing these two equations, the velocity in the vicinity of the walls (boundary layer) is completely different; therefore, this simple equation for the free turbulent jet (Eq. (2)) cannot be used when discussing the velocity in the vicinity of the floor for IJV.

There was a small discrepancy between the measured velocity profiles at Plane-90 and the empirical equations of both Verhoff and the free turbulent jet, assumed to be due to the vertical wall as discussed at Fig. 8. Although the wall could significantly affect the jet, the discrepancy was small, and the jet maintained its self-similarity in the planes at different angles from the wall. Consequently, it is possible to roughly predict the velocity profiles using these equations regardless of the angle.

3.3. Difference by measurement method

The velocity contours under isothermal conditions in the central cross-section obtained by the hotwire anemometer and PIV are compared in Fig. 11. The vertical profiles of radial velocity obtained by the hotwire anemometer and PIV in the central cross-section are compared in Fig. 12. Although the results obtained by the hotwire anemometer are the velocity magnitude in the radial plane, i.e., composite velocity of two components, the results are shown as a form of radial velocity. It is possible to obtain the detailed velocity distribution using the PIV measurement technique; however, the air velocity under the inlet duct is small because there was not sufficient tracer due to the seeding method in the present measurement, as mentioned in Section 2.3.

The maximum radial velocity up to the radial coordinate of 0.4 m is significantly different between the results obtained by PIV and the hotwire anemometer. Since the air in this region is within the core of the jet, it is assumed that the surrounding air, which includes the tracers, cannot be entrained by the jet into this region using the present tracer seeding method (see Section 2.3 for details). Additionally, it is

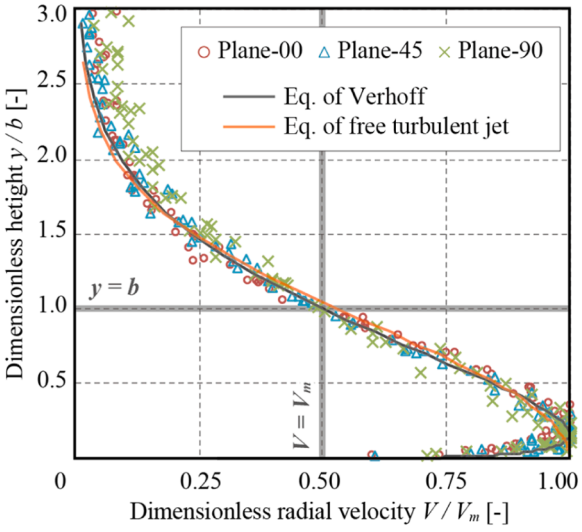

Fig. 10. Vertical profile of Dimensionless radial velocity.

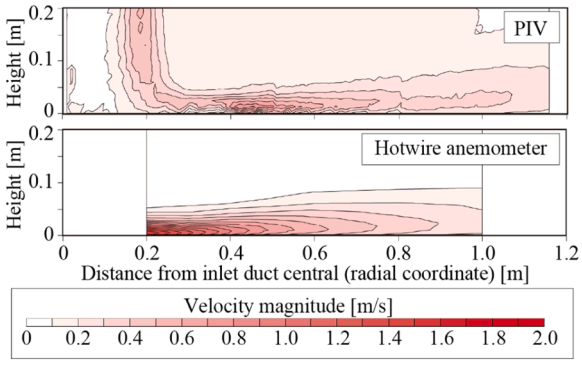

Fig. 11. Comparison of hotwire anemometer and PIV: velocity magnitude distribution in the central cross-section.

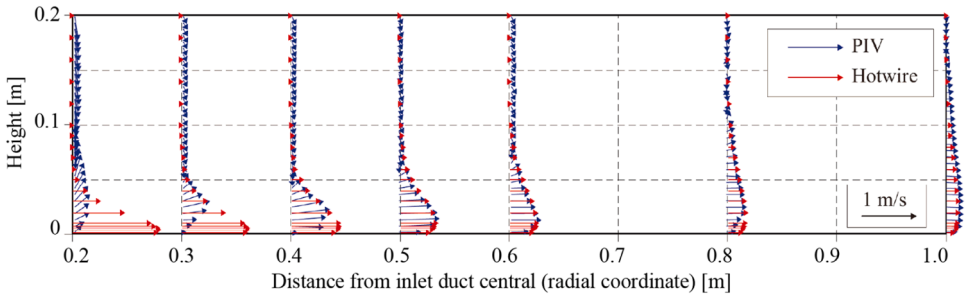

Fig. 12. Comparison of hotwire anemometer and PIV: vertical profiles of radial velocity in the central cross-section.

considered that the jet is not fully developed in the region 0.4 m away from the wall, as mentioned in Section 3.2. On the other hand, the PIV results in the area from the radial distance of 0.5 to 1.0 m from the inlet centre are almost the same as those of the hotwire anemometer. Thus, the PIV with present setups can be used to obtain the velocity profiles in the region far enough from the inlet, i.e., where the jet is fully developed, and the entrainment of the surrounding air occurs. Consequently, the region more than 0.5 m away from the supply terminal centre should be focused on when discussing the PIV results in the following section.

3.4. Influence of temperature settings

The profiles of velocity vectors under isothermal and non-isothermal (cooling) conditions in the central cross-section obtained by the PIV are compared in Fig. 13. According to the discussion in the previous section, the region more than 0.5 m away from the supply terminal centre is to be discussed in the present section.

The jet along the floor is larger in cooling mode. The velocity magnitude is slightly larger in cooling mode than under isothermal conditions; however, the velocity profiles are approximately the same. It is assumed that due to the high density of the cool supplied air, the jet remains close to the floor, resulting in a large flow rate, i.e., high air velocity. Conversely, the airflow adheres to the floor and moves along it because of the jet's momentum under non-isothermal conditions.

In conclusion, the velocity profiles are approximately identical under cooling and isothermal conditions in the present cases. According to these flow features, it is considered that the findings derived under isothermal conditions in Section 3.2 can be applied to the cooling conditions as well.

4. Conclusion

Since the primary feature of the IJV is the impinging jet along the floor, the velocity profiles were measured through a full-scale experiment. Both the hotwire anemometer and PIV were utilised for this measurement. Measurements under isothermal conditions were conducted with the hotwire anemometer and PIV, whereas measurements under non-isothermal conditions were carried out solely by PIV. The velocity profiles at planes with various angles from the central cross-section were also measured using the hotwire anemometer.

The results are discussed in terms of (i) fundamental data of IJV supply jet, (ii) the difference of velocity profiles in the planes with several angles from the central cross-section, (iii) the difference of results measured by the hotwire anemometer and PIV, and (iv) the influence of the temperature settings on the velocity profiles.

(i) The fundamental data of the IJV supply jet

The turbulence statistics of the IJV supply jet are provided. It was shown that the turbulent length scale derived from the autocorrelation in the present study has the same order as 0.07D, which is often used in previous studies.

(i) The angles from the central cross-section

The turbulence statistics of the IJV supply jet are provided. It was shown that the turbulent length scale. The maximum velocity decay and jet half-width expansion differed depending on the angle. Plane-90 (the plane, which is 90° from the central cross section) was very close to the wall; thus, it was affected by the wall in the area close to the supply terminal. The maximum velocity decay was limited in Plane-45 and Plane-90 than in the central cross-section, presumably due to the restriction from the wall. However, when height and velocity are expressed in non-dimensional form, the velocity profiles can be represented by an equation regardless of the angle. In addition, not only the regression curve for the wall jet, but also the regression curve for the free turbulent jet, showed a good agreement with the measured results outside the boundary layer.

(i) The experimental technique

Because of the flow feature of the IJV and the seeding method of the tracer, the measurement accuracy of PIV was lower in the region close to the inlet. However, the results obtained by the hotwire anemometer and PIV were almost the same at the region 0.5 m away from the inlet duct centre, where the jet is presumably fully developed. The PIV results obtained by the present setups must be analysed in the area farther than 0.5 m from the supply inlet duct centre.

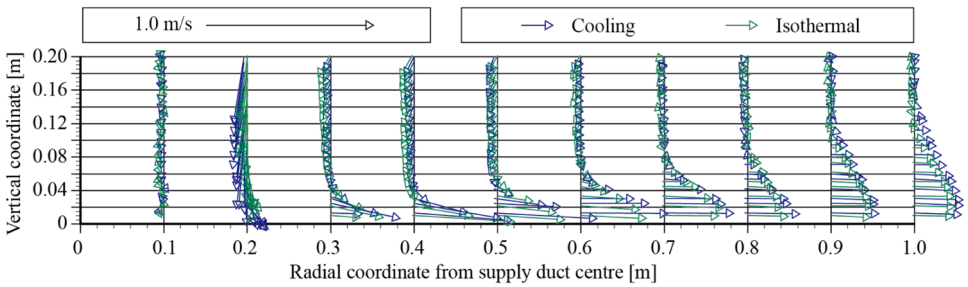

Fig. 13. Velocity vector at the central cross-section (green: isothermal, blue: cooling).

(i) The temperature settings

The velocity was slightly larger under cooling conditions than under isothermal conditions, assumed to be due to the difference in air density, i.e., cool supplied air stayed close to the floor, resulting in a larger velocity. Although the balance between supply momentum and buoyancy was not the same, the velocity profiles were approximately identical under cooling and isothermal conditions in the present cases. It is considered that the regression curves derived under isothermal conditions in Section 3.2 can be applied to the cooling conditions as well.

This study has limitations for the inlet velocity, temperature, and geometrical configuration (discharge height and diameter and shape of duct, and room shape). In addition, since the accuracy of PIV measurement relies on how to seed the tracer, therefore, the seeding method needs to be improved. However, by using these measurement results, it is possible to validate the results by using computational fluid dynamics. After obtaining a validated CFD model based on the experimental measurement, a more detailed CFD simulation, including the evaluation of ventilation effectiveness, can be done as the next step.

CRediT authorship contribution statement

Haruna Yamasawa: Writing – review & editing, Writing – original draft, Visualization, Project administration, Methodology, Investigation, Funding acquisition, Formal analysis, Data curation. **Tomohiro Kobayashi:** Supervision, Resources, Project administration, Conceptualization. **Toshio Yamanaka:** Resources, Methodology. **Narae Choi:** Methodology. **Moe Koshida:** Methodology, Investigation, Data curation.

Declaration of competing interest

This manuscript has not been published or presented elsewhere in part or in entirety and is not under consideration by another journal. We have read and understood your journal's policies, and we believe that neither the manuscript nor the study violates any of these. There are no conflicts of interest to declare.

Acknowledgement

A part of this work was supported by JSPS KAKENHI Grant Number JP20J10608 (Principal Investigator, Haruna Yamasawa). This research did not receive any specific grant from funding agencies in the public, commercial, or not-for-profit sectors.

Data availability

Data will be made available on request.

References

[1] T. Karimipanah, H.B. Awbi, Theoretical and experimental investigation of impinging jet ventilation and comparison with wall displacement ventilation, Build. Environ. 37 (2002) 1329–1342, https://doi.org/10.1016/S0360-1323(01)00117-2.
[2] T. Karimipanah, M. Sandberg, H.B. Awbi, A Comparative Study of Different Air Distribution Systems in a Classroom, Roomvent, Reading (2000) 1013–1018.
[3] T. Karimipanah, H.B. Awbi, M. Sandberg, C. Blomqvist, Investigation of air quality, comfort parameters and effectiveness for two floor-level air supply systems in classrooms, Build. Environ. 42 (2007) 647–655, https://doi.org/10.1016/j.buildenv.2005.10.016.
[4] P. Bradshaw, E.M. Love, The Normal Impingement of a Circular Air Jet On a Flat Surface, 1959. London, https://reports.aerade.cranfield.ac.uk/handle/1826.2/3776.
[5] Y.-G. Tsuei, J.-L. Chao, L.V. Baldwin, Fundamental study of a submerged and non-submerged three dimensional jet impinging upon a normal plane. https://mountainscholar.org/handle/10217/197980, 1963.
[6] M. Poreh, Y.G. Tsuei, J.E. Cermak, Investigation of a Turbulent Radial Wall Jet, J. Appl. Mech. 34 (1967) 457–463, https://doi.org/10.1115/1.3607705.
[7] M.T. Karimipanah, M. Sandberg, Decay of momentum and velocity in an axisymmetric impinging jet, in: Proc. Fourth Int. Conf. Air Distrib. Rooms, 1994.
[8] M.B. Glauert, The wall jet, J. Fluid Mech. 1 (1956) 625, https://doi.org/10.1017/s002211205600041x.
[9] P. Bakke, An experimental investigation of a wall jet, J. Fluid Mech. 2 (1957) 467–472, https://doi.org/10.1017/S0022112057000270.
[10] A. Verhoff, The two-dimensional, turbulent wall jet with and without an external free stream. https://apps.dtic.mil/sti/citations/AD0406073, 1963.
[11] T. Tanaka, E. Tanaka, Experimental Studies of a Radial Turbulent Jet : 2nd Report, Wall Jet on a Flat Smooth Plate, Bull. JSME. 20 (1978) 209–215, https://doi.org/10.1299/jsme1958.20.209.
[12] N. Rajaratnam, Turbulent Jets, Elsevier Science Ltd., Amsterdam, 1976.
[13] F. Canepa, M. Burlando, D. Romanic, G. Solari, H. Hangan, Downburst-like experimental impinging jet measurements at the WindEEE Dome, Sci. Data. 9 (2022) 1–11, https://doi.org/10.1038/s41597-022-01342-1.
[14] J. Varodoumpun, M. Navvab, The impact of terminal configurations in impinging jet ventilated room, in: IAQVEC 2007 Proc. - 6th Int. Conf. Indoor Air Qual. Vent. Energy Conserv. Build. Sustain. Built Environ 3, 2007, pp. 389–396.
[15] J. Varodoumpun, M. Navvab, The full scale and CFD simulation of impinging jet ventilation, in: IAQVEC 2007 Proc. - 6th Int. Conf. Indoor Air Qual. Vent. Energy Conserv. Build. Sustain. Built Environ 3, 2007, pp. 397–404.
[16] T. Kobayashi, K. Sugita, N. Umemiya, T. Kishimoto, M. Sandberg, Numerical investigation and accuracy verification of indoor environment for an impinging jet ventilated room using computational fluid dynamics, Build. Environ. 115 (2017) 251–268, https://doi.org/10.1016/j.buildenv.2017.01.022.
[17] A. Li, L. Gou, X. Wang, Y. Zhang, 2D-PIV experiment analysis on the airflow performance of a floor-based air distribution with a novel mushroom diffuser (FBAD-MD), Energy Build. 121 (2016) 114–129, https://doi.org/10.1016/j.enbuild.2016.03.075.
[18] X. Yang, X. Ye, B. Zuo, K. Zhong, Y. Kang, Analysis of the factors influencing the airflow behavior in an impinging jet ventilation room, Build. Simul. 14 (2021) 749–762, https://doi.org/10.1007/s12273-020-0690-6.
[19] H.J. Chen, B. Moshfegh, M. Cehlin, Numerical investigation of the flow behavior of an isothermal impinging jet in a room, Build. Environ. 49 (2012) 154–166, https://doi.org/10.1016/j.buildenv.2011.09.027.
[20] H.J. Chen, B. Moshfegh, M. Cehlin, Investigation on the flow and thermal behavior of impinging jet ventilation systems in an office with different heat loads, Build. Environ. 59 (2013) 127–144, https://doi.org/10.1016/j.buildenv.2012.08.014.
[21] O. Han, A. Li, Velocity distribution of wall-attached jets in slotted-inlet ventilated rooms, Build. Environ. 194 (2021) 107708, https://doi.org/10.1016/j.buildenv.2021.107708.
[22] X. Yuan, Q. Chen, L.R. Glicksman, A critical review of displacement ventilation, ASHRAe Trans. 104 (1998) 78–90.
[23] E. Mundt, Displacement Ventilation Systems- Convection Flows and Temperature Gradients, Build. Environ. 30 (1995) 129–133, https://doi.org/10.1016/0360-1323(94)E0002-9.
[24] P.V. Nielsen, Displacement Ventilation -Theory and Design, Aalborg University, 1993.
[25] G. Cao, H. Awbi, R. Yao, Y. Fan, K. Sirén, R. Kosonen, J. (Jensen) Zhang, A review of the performance of different ventilation and airflow distribution systems in buildings, Build. Environ. 73 (2014) 171–186, https://doi.org/10.1016/j.buildenv.2013.12.009.
[26] H. Skistad, Displacement Ventilation, Research Studies Press Ltd., 1994.
[27] P.V. Nielsen, The "Family Tree" of Air Distribution Systems. Roomvent 2011, TAPIR Akademisk Forlag, Trondheim, 2011.
[28] H. Yamasawa, T. Kobayashi, T. Yamanaka, N. Choi, M. Matsuzaki, Experimental investigation of difference in indoor environment using impinging jet ventilation and displacement ventilation systems, Int. J. Vent. (2021) 1–18, https://doi.org/10.1080/14733315.2020.1864572.
[29] A. Ameen, M. Cehlin, U. Larsson, T. Karimipanah, Experimental investigation of the ventilation performance of different air distribution systems in an office environment—Cooling mode, Energies 12 (2019) 1354–1368, https://doi.org/10.3390/en12071354.
[30] H. Yamasawa, T. Kobayashi, T. Yamanaka, N. Choi, M. Cehlin, A. Ameen, Applicability of displacement ventilation and impinging jet ventilation system to heating operation, Japan Archit. Rev. 4 (2021) 403–416, https://doi.org/10.1002/2475-8876.12220.
[31] X. Ye, Y. Kang, X. Yang, K. Zhong, Temperature distribution and energy consumption in impinging jet and mixing ventilation heating rooms with intermittent cold outside air invasion, Energy Build. 158 (2018) 1510–1522, https://doi.org/10.1016/j.enbuild.2017.11.038.
[32] X. Ye, Y. Kang, F. Yang, K. Zhong, Comparison study of contaminant distribution and indoor air quality in large-height spaces between impinging jet and mixing ventilation systems in heating mode, Build. Environ. 160 (2019) 106159, https://doi.org/10.1016/j.buildenv.2019.106159.
[33] X. Ye, Y. Kang, B. Zuo, K. Zhong, Study of factors affecting warm air spreading distance in impinging jet ventilation rooms using multiple regression analysis, Build. Environ. 120 (2017) 1–12, https://doi.org/10.1016/j.buildenv.2017.03.044.
[34] H. Yamasawa, T. Kobayashi, T. Yamanaka, N. Choi, M. Cehlin, A. Ameen, Effect of supply velocity and heat generation density on cooling and ventilation effectiveness in room with impinging jet ventilation system, Build. Environ. 205 (2021) 108299, https://doi.org/10.1016/j.buildenv.2021.108299.
[35] X. Ye, Y. Kang, F. Yang, K. Zhong, Comparison study of contaminant distribution and indoor air quality in large-height spaces between impinging jet and mixing

ventilation systems in heating mode, Build. Environ. 160 (2019) 106159, https://doi.org/10.1016/j.buildenv.2019.106159.
[36] A. Staveckis, A. Borodinecs, Impact of impinging jet ventilation on thermal comfort and indoor air quality in office buildings, Energy Build. 235 (2021) 110738, https://doi.org/10.1016/j.enbuild.2021.110738.
[37] C. Qin, S.S. Cai, X. Lyu, W.Z. Lu, Cross transmission of normal breathing-released contaminants in a general hospital ward with impinging jet supply: a numerical study, J. Build. Eng. 92 (2024) 109766, https://doi.org/10.1016/j.jobe.2024.109766.
[38] B. Yang, P. Liu, Y. Liu, F. Wang, Performance evaluation of ductless personalized ventilation combined with impinging jet ventilation, Appl. Therm. Eng. 222 (2023) 119915, https://doi.org/10.1016/j.applthermaleng.2022.119915.
[39] T. Duan, X. Ye, P. Du, H. Qi, Y. Kang, K. Zhong, Study of indoor local thermal comfort for impinging jet ventilation combined with ductless personalized ventilation under different cooling loads, Build. Environ. 265 (2024), https://doi.org/10.1016/j.buildenv.2024.112013.
[40] A. Ameen, M. Cehlin, U. Larsson, H. Yamasawa, T. Kobayashi, Numerical Investigation of the Flow Behavior of an Isothermal Corner Impinging Jet for Building Ventilation, Build. Environ 223 (2022) 109486, https://doi.org/10.1016/j.buildenv.2022.109486.
[41] H. Kotani, T. Kobayashi, Accuracy verification of processing methodology in particle image velocimetry for flow around building, J. Environ. Eng. (Transactions AIJ). 80 (2015) 741–749, https://doi.org/10.3130/aije.80.741.
[42] R.D. Keane, R.J. Adrian, Theory of cross-correlation analysis of PIV images, Appl. Sci. Res. 49 (1992) 191–215, https://doi.org/10.1007/BF00384623.
[43] C.E. Willert, M. Gharib, Digital particle image velocimetry, Exp. Fluids. 10 (1991) 181–193, https://doi.org/10.1007/BF00190388.
[44] T. Kobayashi, K. Sagara, T. Yamanaka, H. Kotani, M. Sandberg, Wind driven flow through openings - Analysis of the stream tube, Int. J. Vent. 4 (2006) 323–336, https://doi.org/10.1080/14733315.2005.11683712.
[45] D.C. Wilcox, Chapter 4 - One-Equation and Two-Equation Models. Turbul. Model. CFD, Third, 1933, pp. 107–238. San Diego.